Published in final edited form as:
Expert Syst Appl. 2012 June 15; 39(8): 7355–7370. doi:10.1016/j.eswa.2012.01.071.

Mapping and mining interictal pathological gamma (30–100 Hz) oscillations with clinical intracranial EEG in patients with epilepsy

Otis Smart[a,b,*], **Douglas Maus**[c], **Eric Marsh**[d], **Dennis Dlugos**[d], **Brian Litt**[e], and **Kimford Meador**[f]

[a]Intelligent Control Systems Laboratory, Georgia Institute of Technology, Atlanta, GA 30332, USA

[b]Department of Neurosurgery, Emory University, Atlanta, GA 30322, USA

[c]Department of Neurology, SUNY Downstate Medical Center, Brooklyn, NY 11203, USA

[d]Division of Neurology, Children's Hospital of Philadelphia, Philadelphia, PA 19104, USA

[e]Departments of Neurology and Bioengineering, University of Pennsylvania, Philadelphia, PA 19104, USA

[f]Department of Neurology, School of Medicine, Emory University, Atlanta, GA 30322, USA

Abstract

Localizing an epileptic network is essential for guiding neurosurgery and antiepileptic medical devices as well as elucidating mechanisms that may explain seizure-generation and epilepsy. There is increasing evidence that pathological oscillations may be specific to diseased networks in patients with epilepsy and that these oscillations may be a key biomarker for generating and indentifying epileptic networks. We present a semi-automated method that detects, maps, and mines pathological gamma (30–100 Hz) oscillations (PGOs) in human epileptic brain to possibly localize epileptic networks. We apply the method to standard clinical iEEG (<100 Hz) with interictal PGOs and seizures from six patients with medically refractory epilepsy. We demonstrate that electrodes with consistent PGO discharges do not always coincide with clinically determined seizure onset zone (SOZ) electrodes but at times PGO-dense electrodes include secondary seizure-areas (SS) or even areas without seizures (NS). In 4/5 patients with epilepsy surgery, we observe poor (Engel Class 4) post-surgical outcomes and identify more PGO-activity in SS or NS than in SOZ. Additional studies are needed to further clarify the role of PGOs in epileptic brain.

Keywords

Epileptic network; Interictal epileptic discharge; Pathological gamma oscillation; Detection; Mapping; Data-mining

*Corresponding author. Address: Emory University, Woodruff Memorial Research Building, 101 Woodruff Circle, Room 6329, Atlanta, GA 30322, USA., otissmart@gmail.com (O. Smart).

7. Disclosures

No conflicts of interest, financial or otherwise, are declared by the author(s).

1. Introduction

Epilepsy is a neurological disorder that is characterized by recurrent, unprovoked seizures (Destexhe, Contreras, Sejnowski, & Steriade, 1994). Because a seizure is a strong synchronous surge of electrical activity in the brain, it disrupts the normal functioning of the brain and may cause one or more adverse physical symptoms for an unpredictable period of time. Thus, seizures and the threat of having a seizure can debilitate the quality of life for a person with epilepsy by affecting many aspects of their lives, including their health, finances, relationships, social activities, employment, and personal morale. Fortunately, with the appropriate treatment to control or eliminate seizures, it is possible to improve quality of life in many people who suffer from epilepsy.

Neurosurgery is a safe and effective treatment for patients with medically refractory epilepsy (Spencer et al., 2003, 2007; Tanriverdi, Ajlan, Poulin, & Olivier, 2009; Tanriverdi, Poulin, & Olivier, 2008; Wiebe, Blume, Girvin, Eliasziw, & the Effectiveness and Efficiency of Surgery for Temporal Lobe Epilepsy Study, 2001), a condition in which medical drugs cannot adequately control epileptic seizures (French et al., 2004; Wiebe et al., 2001). The goal of neurosurgery is to remove the epileptogenic zone (EZ), or the neural tissue that necessarily generates epileptic seizures (Engel, 1996; Rosenow & Luders, 2001), without removing or damaging the critical brain for neurological or neuropsychological functions. Although non-invasive evaluations (e.g., scalp EEG, MRI) may be used for localizing the EZ, many patients require invasive electroencephalography (EEG)—the measurement of electrical activity from the brain via surgically implanted electrodes—to estimate the location and extent of the EZ. To prepare for neurosurgery, such patients are hospitalized in an epilepsy monitoring unit (EMU) where invasive EEG, or intracranial EEG (iEEG), is clinically monitored and continuously recorded to electrographically capture epileptic activity that may help identify the EZ and direct the appropriate surgery. That is, the iEEG is visually screened by epileptologists and clinicians to find ictal activity (seizures) or brief paroxysmal interictal activity (transient discharges between seizures) that may likely indicate considerably diseased brain for treatment.

Recent research using recording iEEG at high bandwidth (i.e., maximum frequency of 1000–9000 Hz) in patients with epilepsy strongly suggests that the iEEG contains a particular biomarker of the EZ or at least the seizure onset zone (SOZ), a supposed subarea of the EZ. This biomarker, which is known as a pathological high-frequency oscillation (pHFO) or alternatively as a fast ripple (FR), is characterized as a very brief, low-amplitude high-gamma (200–500 Hz) activity that is visible on microelectrode or macroelectrode iEEG in patients with neocortical or mesial temporal lobe epilepsy after keen visual inspection or digital filtration of the iEEG (Bragin, Engel, Wilson, Fried, & Buzsaki, 1999; Bragin, Engel, Wilson, Fried, & Mathern, 1999; Bragin, Mody, Wilson, & Engel, 2002; Bragin, Wilson, et al., 2002; Buzsaki, Horvath, Urioste, Hetke, & Wise, 1992; Contreras, Destexhe, & Steriade, 1997; Jacobs et al., 2008; Jirsch, Chander, & Gotman, 2007; Jirsch et al., 2006; Staba, Wilson, Bragin, Fried, & Engel, 2002; Urrestarazu, Chander, Dubeau, & Gotman, 2007; Worrell et al., 2008). Unfortunately, despite such interesting and compelling research on pHFOs, epilepsy monitoring units (EMUs) of most hospitals still conventionally collect clinical iEEG at relatively low limited bandwidth (i.e., maximum frequency of 70–100 Hz) compared to the experimental protocols of human studies. This restriction in recording iEEG is due to either the lack of appropriate equipment or the considerably increased costs of storing and securing such larger amounts of high-bandwidth data. However, a correlation between pathological oscillations and the EZ may not be restricted to only frequencies above 100 Hz with previous literature having observed epileptic activity within the iEEG of patients at a lower traditional gamma band (30–100 Hz). For instance, using clinical iEEG in patients with neocortical epilepsy, Worrell and collaborators (Worrell et al., 2004)

previously report gamma (60–100 Hz) oscillations, 'high frequency epileptiform oscillations (HFEOs),' that are highly localized in the SOZ of patients with neocortical epilepsy. We refer to such epileptic activity as pathological gamma oscillations (PGOs) since its spectral content is actually lower in than the higher bandwidth of pHFOs. There does not appear to be much literature that studies the relationship between 60 and 100 Hz PGOs and the SOZ in patients with intractable temporal lobe epilepsy.

Furthermore, because the iEEG in a presurgical evaluation for neurosurgery is measured from multiple sites (electrodes) in the brain (where the presumption is that more sites may provide better spatial resolution in estimating the EZ), it would be of great clinical value if PGOs could be exploited to determine (1) which sites are most essentially involved with the EZ—we call this task mapping, (2) whether there exists a reliable organization or interconnection of these sites—we call this task mining; and (3) whether removing brain regions that generate this network of aberrant activity can improve the outcome of epilepsy surgery. Previous studies already suggest that the EZ is actually a pathological network of tissue, which can generate ictal and interictal hypersynchronous discharges most likely through a mechanism that mimics kindling (Badier & Chauvel, 1995; Bartolomei, Wendling, Bellanger, Regis, & Chauvel, 2001; Bragin, Wilson, & Engel, 2000). Yet limited work currently exists on objectively deriving an epileptogenic network with iEEG PGOs. While recent research estimates epileptogenic networks by analyzing the spatial–temporal distribution of interictal epileptic activity (Bourien, Bellanger, Bartolomei, Chauvel, & Wendling, 2004), no reported studies yet investigate the relationship between analyzed spatial–temporal information and the SOZ, the surgically removed tissue (which is the projected EZ), or post-surgical outcomes. We suggest that such studies may form the basis for a presurgical clinical test that reliably predicts the EZ and permits the most effective neurosurgical treatment.

Lastly, because PGOs occur intermittently within many continuously recorded signals over several days, correctly mapping and mining epileptic networks are highly complex and practically impossible tasks for even the most experienced epileptologist to accomplish, especially via only visual screening. Therefore this test requires efficient user-friendly algorithms to analyze the iEEG and predict the most epileptogenic foci. We describe a general framework, which may be adapted across different bands of frequencies and epileptic activity, for semi-automatically detecting, mapping, and mining potential epileptic networks. We apply the technique to pathological gamma oscillations within clinical recordings of multielectrode intracranial EEG. The framework sequentially combines automated algorithms for pattern detection previously developed by our group to identify oscillations and pattern recognition using frequent itemset mining (FIM) to identify electrodes where these oscillations cluster over time. FIM is a well-known technique in the field of machine-learning and can be used to objectively discern the reproducibility of complex patterns within a large volume of data. We discuss FIM in more detail in the appendix but refer to it as a 'black-box' in other sections of this work.

2. Methods

2.1. Patients

We analyzed iEEG signals from six patients with medically refractory temporal lobe epilepsy who underwent long-term continuous video-EEG monitoring for presurgical evaluation at Emory University (EU) and the Children's Hospital of Philadelphia (CHP). Each patient provided informed consent for participation in research studies under the approval of the Internal Review Boards (IRBs) at EU and CHP. Hospital stays varied from 3 to 27 days for the patients.

2.2. Electrodes

According to standard clinical protocols for presurgical evaluation (Engel, 1987), patients were implanted with subdural and depth electrodes that were manufactured by Ad-Tech Medical Instrument Corporation (Racine, WI). The total number of electrodes per patient depended upon the clinical requirements for presurgical evaluation. Each subdural electrode was a platinum disc (4.0 mm total diameter with ~2.3 mm diameter exposed) and 4–6 electrodes were arranged in a single strip (10.0 mm center-to-center spacing). Each depth electrode was a platinum cylinder (~1.1 mm diameter, ~2.4 mm length) and 6 electrodes were arranged as a single part (~10 mm center-to-center spacing).

2.3. Data: digital acquisition

For each EU patient, continuous iEEG were collected with a 64- channel Nicolet BMSI-5000 digital EEG system (Nicolet Biomedical, Madison, WI), which incorporated an analog Butterworth bandpass anti-aliasing filter (cutoffs −3 dB at 0.5 and 150 Hz), then digitization at 12 bits per sample and 400 samples per second before digital low-pass filtering (−3 dB cutoff at 100 Hz) and down-sampling to 200 samples per second for final storage. For the one CHP patient, continuous iEEG were recorded with a 128-channel Grass-Telefactor system, which incorporated an analog anti-aliasing bandpass filter (−3 dB cutoffs at 0.5 and 100 Hz), digitization at 12 bits per sample and 800 samples per second before digital low-pass filtering (−3 dB cutoff at 70 Hz) and down-sampling to 200 samples per second for final storage.

2.4. Data: selection and documentation

For each patient, the ensuing procedures were performed. All recorded iEEG signals were visually reviewed for seizures and pathological gamma oscillations. The time of the earliest iEEG change and the associated electrode(s) were defined as the electrographic seizure onset time (SOT) and seizure onset zone (SOZ), respectively. More specifically, the SOT and SOZ were determined by independent visual identification of a clear ictal discharge in the iEEG before looking backward in the recording for the earliest definite change that was contiguously associated with the seizure. Non-SOZ electrodes were categorized as either ‘seizure-spread’ (SS), meaning sites with apparent secondary clinical or electrographic discharge, or ‘no seizure’ (NS), meaning sites with no apparent clinical or electrographic discharge. We recorded the SOT and all labeled electrodes per seizure in an Excel (Microsoft, Redmond, WA) spreadsheet as a reference for statistical analyses. Additionally, we noted the post-surgical outcome (Engel, Van Ness, Rasmussen, & Ojemann, 1993) of each patient at 12–15 months and over 2 years.

We prepared two separate samples of manually clipped signals using the collected iEEG: a training dataset (n = 8–15) for tuning the algorithm to detect PGOs (see ‘Automated Detection) and a testing dataset (n = 4–14) for executing the algorithms to spatially map (see ‘Automated Mapping’) and spatiotemporally mine (see ‘Automated Mining’) PGOs. We used the following criteria to prepare the training dataset: (1) clips of interictal iEEG (~2–4 min) were taken at least 5 min before a seizure; (2) a clip was selected from any one electrode but not necessary the same electrode in repeated selections; (3) a clip was ~2 min in duration with at least 40 ‘gold standard’ PGOs; (4) the clips were not chosen using the information in the Excel document. We used the following criteria to prepare the testing dataset: (1) clips of interictal iEEG (CHP: ~30 min, EU: ~60 min) were taken beginning at least 65 min before a seizure; (2) all recorded electrodes were included in a clip and electrodes with artifacts were later discarded before statistical analyses; (3) each clip contained PGOs. We also referred to each clip in the testing dataset as an interictal record. Fig. 1 illustrates PGOs within a testing clip and the ictal activity that immediately followed the interictal record.

2.5. Automated detection

The designed semi-automated algorithm to mark iEEG PGOs implemented previously validated algorithms (Gardner, Worrell, Marsh, Dlugos, & Litt, 2007; Kahane et al., 1999) to detect interictal oscillations. The custom MATLAB algorithm sequentially incorporated high-pass filtration (−3 dB cutoff at 30 Hz, Chebychev filter), normalization of the filtered signals using a non-parametric z-scoring (i.e., median and spread rather than mean and deviation, respectively), extraction of the feature "line-length" (Esteller, Echauz, & Tcheng, 2004) with 75% overlap between consecutive 100 ms windows of normalized filtered data, and binary classification of the extracted feature-values using a binary threshold (i.e., values above or equal to the threshold were assigned a label of one and values below the threshold were assigned a label of zero). The transition from low (0) to high (1) and high to low were respectively registered as the beginning and ending time-stamps of the detected event while the corresponding electrode on which the detector triggered was co-registered as the detected channel.

The window for extracting the feature and the threshold for classification were empirically determined using the training data (see 'Data: Selection & Documention') after the time-stamps and channel of every PGO in the sample were manually marked and automatically stored using a MATLAB (Mathworks, Natick, MA) graphical user interface (GUI) (Gardner et al., 2007). The window for each patient was determined by computing the minimum duration of PGOs. The threshold for each patient was determined using an analysis that combined a receiver operating characteristic (ROC) curve and hypothesis-testing (see 'Appendix A'). Essentially, we computed a threshold with high selectivity that tolerated false positives and false negatives of the detector without considerably changing the results of mapping and mining the detections.

2.6. Automated mapping

In our context, analyzing interictal epileptic activity in iEEG, we defined *spatial mapping* (or just *mapping*) as registering the density of interictal epileptic activity relative to the location of the implanted electrodes using a measurement of the activity. The automated algorithm to spatially map PGOs performed three main operations: (1) imported the results of the semi-automated detection; (2) computed for each electrode at least one measurement (e.g., rate of occurrence, median energy, mean entropy) from the detected events, and (3) normalization of the measurement in operation (2) by $2(x_i - \tilde{x})/iqr(x)$, where x_i is the measurement on electrode i, $\tilde{x}$ is the median measurement across all electrodes, and $iqr(x)$, is the inter-quartile range of all measurements.

Optionally, a supplementary MATLAB GUI plotted the results of the mapping as (1) a histogram with the labels for the electrodes on the y-axis and the measurement (native or normalized value) on the x-axis and/or (2) a brain-plot, using a user-imported referential image of the brain, with superimposed dots that represented the locations of the surgically implanted electrodes (e.g., blue dots) and the locations of mapped PGOs (e.g., red dots). The GUI plotted the results for each interictal record, allowing the user to scroll through a number of selected records.

2.7. Automated mining

In addition, we defined *spatial mining* (or just *mining*) of interictal iEEG activity as registering the density of interictal epileptic activity (or a measure of the activity) that represents a potential network of connected pathological brain relative to the location of the implanted electrodes. The algorithm to mine PGOs (and putatively identify epileptic networks) was a custom MATLAB program that sequentially performed three main operations: (1) computed a spatial–temporal matrix of measurements from the detected

events by extracting at least one preselected feature for each detected event, using a single statistic (e.g., median, sum) to reduce the multiple measured events to a single measurement, and organizing the measurements in a matrix for which each row corresponded to a 1 min window of events while each column corresponded to the electrode of the quantified event; (2) executed a binary rule for each row of the matrix to classify and group the electrodes per row (segment of time); and (3) executed an efficient C++ (Microsoft Visual Studio, Redmond, WA) algorithm for frequent itemset mining (FIM) (Bodon, 2005), where the FIM was repeated with a few distinct levels of support (see 'Primary Analyses' and 'Appendix B'). The binary rule was arbitrary since we could not a priori know the epileptic network to set a threshold, but we defined a requirement such that columns (electrodes) with values greater than or equal to a threshold were made zero (0) and values less than the threshold were made one (1). A raster-plot of the largest subset of maximally reproducible mined electrodes as a function of reproducibility (level of support) was generated (results not here shown).

Optionally, a supplementary MATLAB GUI plotted the results of the mining as a raster-plot with the labels for the electrodes on the y-axis, the level of support on the x-axis, and a dot at each x–y pair where the FIM discovered a frequent item. In addition, the GUI plotted the results of the mining on a brain-plot, using a user-imported referential image of the brain, with superimposed dots that represented the locations of the surgically implanted electrodes (e.g., blue dots) and the locations of mined PGOs (e.g., red dots). The GUI plotted the results for each interictal record, allowing the user to scroll through a number of selected records, including controls for the user to select and view the FIM results for each combination of support and number of mined electrodes at that support.

2.8. Primary analyses & statistics: quantifying, mapping, and mining oscillations

For each patient, we conducted three main experiments using the training and testing datasets as conceptually illustrated in Fig. 2: (1) quantifying or characterizing pathological gamma oscillations by using the training dataset (Fig. 2B); (2) mapping pathological gamma oscillations by individually using two selected measures (i.e., average rate and average energy) of the detected events within the testing dataset (Fig. 2C); and (3) mining pathological gamma oscillations by individually using two selected measures (i.e., average rate and average energy) of the detected events within the testing dataset (Fig. 2C). We executed each primary analysis with custom MATLAB algorithms. We performed statistical tests for the results of the algorithms using MATLAB and SPSS. For all statistical tests, we considered a computed p-value less than 0.050 a statistically significant observation.

For the first analysis, a sample (n = 200) of PGO events was taken from the entire registrar of manually marked PGOs in the training dataset for each patient. Each PGO event was quantified by four measures: (1) the root-mean-square amplitude; (2) the duration, which we defined as the difference in time between the stored time-stamps; (3) the frequency that corresponded to the peak magnitude of a spectrogram (in the bandwidth of interest), which was computed using the continuous wavelet transformation and a complex Morlet wavelet; (4) the phase that corresponded to the frequency in (3). For each of the four quantities, we pooled all 200 measures for all patients to compute histograms and central tendencies (i.e., mean with standard error of the mean and median) with the appropriate binning (Roederer, Treister, Moore, & Herzenberg, 2001).

For the second analysis, we executed the mapping algorithm for each interictal record to determine the spatial distribution of interictal PGOs using two individual measures to compute the spatial–temporal matrix: (1) count, an intuitively basic feature with low computational burden—this measure was computed directly from the registry of detections with no need to access the auto-marked iEEG; and (2) median energy, since gamma energy

was suggested to possibly distinguish epileptic and relatively normal regions of brain in both neocortical (Urrestarazu et al., 2007; Worrell et al., 2004) and mesial temporal lobe epilepsy (Urrestarazu et al., 2007). For each measure, an omnibus non-parametric repeated-measures test (Friedman test) and post-hoc non-parametric paired tests (Wilcoxon sign-rank tests) analyzed patient-specific mappings to investigate whether the measurement differs between SOZ, SS, and NS electrodes.

For the third analysis, we executed the mining algorithm at nine distinct thresholds (FIM supports or levels of reproducibility, see 'Appendix B') (i.e.,) $\lambda_i = (0.10i,\ 1 \leq i \leq 9)$ and a constant arbitrary threshold for classification (i.e., CHP: 87.5th percentile, others: 75th percentile) for each interictal record per patient. We used a higher threshold for classification for the pediatric data than the adult data because the pediatric patient was implanted with more electrodes and we wanted to equally fix the potential maximum number of mined electrodes for all patients.

We evaluated the statistical significance of each resulting mined electrodes with a multivariate contingency table. For statistically significant mined electrodes, an omnibus one-sample chi-squared test and post-hoc one-sample chi-squared tests analyzed whether the mined electrodes mostly occurred in the SOZ, SS, or NS.

3. Results

3.1. Quantifying pathological gamma oscillations

We quantified the amplitude, frequency, duration, and phase of 4800 manually marked PGOs in the iEEG recordings of all six patients using the training dataset and produced histograms (Fig. 3). From each of the four histograms, we calculated measures of central tendency: amplitude (mean: 10.300 ± 0.187 mV, median: 8.779 mV), frequency (mean: 48.5832 ± 0.7375 Hz, median: 41.861 Hz), duration (mean: 435.073 ± 9.028 ms, median: 361.396 ms), and normalized phase (mean: −0.010 ± 0.020, median: 0.029). Overall, the PGOs were very low-amplitude, low-frequency, brief events in the iEEG.

3.2. Detecting pathological gamma oscillations

We tabulated (Table A1) the performance and threshold of a conventionally tuned detector and a robustly tuned detector, using the ROC curve and hypothesis-testing, for each patient (Fig. A1). The two thresholds differed in each case, resulting in different performances. The latter approach returned thresholds for higher selectivity than sensitivity in detection, and the former approach returned thresholds with either higher or lower selectivity than sensitivity.

3.3. Mapping pathological gamma oscillations

We analyzed the spatial distribution of the mapped PGOs relative to the seizure onset zone, the seizure spread, and areas where no seizure occurred using each the average rate and the average median energy of detected interictal PGOs. Fig. 3 illustrated the results of the mapping algorithm for the second and sixth interictal records from Patient C (Fig. 3A1–B2) and Patient F (Fig. 3C1–D2). Figs. 5 and 6 summarized the results for all patients. We did not execute an omnibus test for Patient F because whose data presented only two categories (i.e., SOZ, SS). But a Wilcoxon sign-rank test showed no statistically difference between the SOZ and the SS for both the average rate (SOZ: mean = 5.85 ± 1.52/min, median = 4.29/min; SS: mean = 7.22 ± 1.35/min, median = 6.39/min; $p_F = 0.236$) and the average energy (SOZ: mean = 222.42 ± 28.84 μV^2, median = 175.22 μV^2; SS: mean = 228.82 ± 19.63 μV^2, median = 223.58 μV^2; $p_F = 0.074$). The omnibus tests found a statistically significant difference in average rate between at least one pair of categories for 3 of the 6 remaining cases (3/5 patients) ($p_A = 0.025$, $p_B = 0.074$, $p_{C1} = 0.034$, $p_{C2} = 0.223$, $p_D = 0.039$, $p_E =$

0.368) and a statistically significant difference in average median energy between at least one pair of categories for 2 of the 6 remaining cases (2/5 patients) ($p_A = 0.018$, $p_B = 0.015$, $p_{C1} = 0.223$, $p_{C2} = 0.846$, $p_D = 0.472$, $p_E = 0.236$).

Post-hoc tests suggested higher average rates in the SOZ vs. NS for patients A, D, and E but statistical significance for only Patient A ($p_A = 0.023$, $p_B = 0.225$, $p_{C1} = 0.050$, $p_{C2} = 0.249$, $p_D = 0.068$, $p_E = 0.059$). Post-hoc tests found no difference in average rate between the SOZ and the SS for any of the patients ($p_A = 0.753$, $p_B = 0.075$, $p_{C1} = 0.050$, $p_{C2} = 0.401$, $p_D = 0.144$, $p_E = 0.173$). The average rates for the SS and the NS did not statistically differ for all patients except patients A and B ($p_A = 0.016$, $p_B = 0.043$, $p_{C1} = 0.674$, $p_{C2} = 0.116$, $p_D = 0.068$, $p_E = 0.374$).

Post-hoc tests for only Patient A demonstrated a statistical difference in average median energy between the categories with the most energy in the SOZ, lesser energy in the SS, and the least energy in NS (SOZ: mean = 941.77 ± 160.22 μV^2, median = 1027.58 μV^2; SS: mean = 764.40 ± 87.83 μV^2, median = 795.61 μV^2; NS: mean = 517.09 ± 43.97 μV^2, median = 448.08 μV^2; SOZ vs. NS: $p_F = 0.039$; SS vs. NS: $p_F = 0.016$; SOZ vs. SS: $p_A = 0.064$). For Patient B, more energy was distributed in the SOZ than the NS (SOZ: mean = 473.82 ± 156.73 μV^2, median = 291.66 μV^2; NS: mean = 233.14 ± 68.57 μV^2, median = 169.45 μV^2; $p_B = 0.043$) but no clear differences in the other pairings (SS vs. NS: $p_F = 0.080$; SOZ vs. SS: $p_A = 0.345$). Except for SOZ vs. NS in Patient C1 (SOZ: mean = 194.61 ± 28.18 μV^2, median = 179.47 μV^2; NS: mean = 272.40 ± 48.56 μV^2, median = 245.04 μV^2; $p_{C1} = 0.017$), post-hoc tests ($n = 13$, $p > 0.093$) for Patients B–E did not demonstrate statistical significance.

Overall, we noticed an inconsistent relationship between the areas of ictal onset and the measure average median energy but a somewhat consistent relationship between the areas of ictal on-set and the measure average rate.

3.4. Mining pathological gamma oscillations

We analyzed the spatial distribution of the mined PGOs relative to the seizure onset zone, the seizure spread, and areas where no seizure occurred using each the average rate and the median energy measures, but discussed results for the former measure since the results of the mapping algorithm with the median energy of detected interictal PGOs did not produce many statistically significant results. Fig. 4 illustrated the results of the mining algorithm for the second and sixth interictal records from Patient C (Fig. 4A1–B2) and Patient F (Fig. 4C1–D2). Fig. 7 summarized the results for all patients. We noticed that mined PGOs mainly localized in electrodes with seizure spread or no seizures (Fig. 7), excluding the iEEG from Patient D, which demonstrated clustered electrodes in mainly either the SOZ or SS, and Patient E, which presented an even distribution of mined PGOs in SOZ, SS, and NS for lower FIM supports (values < 0.50) and mined PGOs in either SOZ or SS for higher FIM supports. For patients other than D and E, varying the FIM support did not considerably change the corresponding findings.

The omnibus test found a statistically significant difference in counted mined electrodes between at least one pair of categories for all patients at certain FIM supports ($p_A < 0.026$: $0.10 < \lambda < 0.90$, $p_B < 0.022$: $0.10 < \lambda < 0.40$, $p_{C1} < 0.021$: $0.10 < \lambda < 0.50$, $p_{C2} < 0.013$: $0.10 < \lambda < 0.20$, $p_D < 0.032$: $0.10 < \lambda < 0.30$, $p_E > 0.206$: $0.10 < \lambda < 0.80$, $p_F < 0.001$: $0.10 < \lambda < 0.90$). Post-hoc tests suggested higher counts in the SS vs. SOZ for patients A, B, C1, C2, and F ($p_A < 0.013$: $0.10 < \lambda < 0.90$, $p_B < 0.007$: $0.20 < \lambda < 0.30$, $p_{C1} < 0.007$: $0.30 < \lambda < 0.50$, $p_{C2} < 0.003$: $0.10 < \lambda < 0.20$, $p_D > 0.317$: $0.10 < \lambda < 0.30$, $p_E > 0.194$: $0.10 < \lambda < 0.80$, $p_F < 0.001$: $0.10 < \lambda < 0.90$), higher counts in the NS than SOZ for patients all patients except D (lower counts in NS vs. SOZ) and both E and F (no difference) ($p_A < 0.007$: $0.10 <$

$\lambda < 0.90$, $p_B < 0.020$: $0.20 < \lambda < 0.30$, $p_{C1} < 0.007$: $0.30 < \lambda < 0.50$, $p_{C2} < 0.020$: $0.10 < \lambda < 0.20$, $p_D < 0.035$: $0.20 < \lambda < 0.30$, $p_E > 0.257$: $0.10 < \lambda < 0.80$, $p_F < 0.257$: $0.10 < \lambda < 0.90$), and typically no difference in counts between SS and NS except for patents A (more counts in NS than SS) and both D and F (more counts in SS than NS) ($p_A < 0.002$: $0.10 < \lambda < 0.50$, $p_B > 0.102$: $0.20 < \lambda < 0.30$, $p_{C1} < 0.274$: $0.10 < \lambda < 0.50$, $p_{C2} < 0.182$: $0.10 < \lambda < 0.20$, $p_D < 0.035$: $0.10 < \lambda < 0.50$, $p_E > 0.077$: $0.10 < \lambda < 0.80$, $p_F < 0.001$: $0.10 < \lambda < 0.90$). Overall, we determined that mined PGOs cluster in all areas of the brain but mostly in the SS and/or NS compared to the SOZ.

4. Discussion

Overall, we demonstrated the potential utility of coupling quantitative techniques in pattern detection (e.g., PGOs) and pattern recognition (e.g., data-mining, data-mapping) to identify pathological networks of tissue in patients with epilepsy. Five of the six patients had epilepsy surgery but only 1 of the 5 patients (the pediatric patient) became seizure-free. In all surgeries, only the clinical SOZ was resected but the computed SOZ using the mapping and mining algorithms to analyze interictal PGOs did not exclusively include the clinical SOZ, pinpointing more areas in the SS or even the NS than the SOZ. In this particular study, the presented algorithms analyzed PGOs but the algorithms have a general computational framework for processing alternate biomarkers of epilepsy.

4.1. Detection

Previously, we designed algorithms for detecting and categorizing of PGOs. But using these techniques in practical systems to automatically identify epileptic networks required that the algorithms demonstrate robustness. That was, the detection algorithm analyses that processed the detections did not return spurious information due to the errors of detection (i.e., false positives and false negatives). We presented a probabilistic ROC analysis as a unique approach to design a detector that provided robust tolerance against false positives and false negatives by subsequent analyses. The probabilistic ROC safeguarded against obscured results from either the mapping or the mining due to the inevitable spurious information (false positives) and lack of information (false negatives) during automatic detection.

Alternatively, we considered executing the automatic detector at a very high sensitivity (low threshold) to avoid losing information and afterward discarding any unavoidable spurious information before subsequent analyses, reintroducing the need for more expert visual inspection of data. However, we devised an approach that avoided further manual screening of iEEG information.

4.2. Mapping and mining

Mapping was an intuitive approach for investigating whether certain electrodes demonstrated extreme rates of PGOs relative to all electrodes over all time. We hypothesized that very high PGO-rates (values greater than a threshold) identified epileptogenic networks. FIM was an appropriate scheme for investigating whether groups (subsets) of electrodes repeatedly co-exhibited PGOs within some short window of time. We hypothesized that patterns of spatiotemporally associated electrodes (sites of brain) identified epileptogenic networks that were signaled by PGOs. We supposed that the input to the mining algorithm (the spatial–temporal matrix) represented time-varying clusters of electrodes that may constitute an epileptic network. When applied, the complete algorithm processed an interictal record and returned the electrodes that consistently exhibited synchronized concentrations of pathological activity.

We showed that both mapping and mining (FIM) yielded clusters of electrodes that did not always include the SOZ but more often identified regions in the SS or even the NS despite differences in the results of each algorithm (cf., Figs. 3 and 4). This finding seemingly contradicted a common hypothesis that epileptic networks must be predominantly located in the SOZ than the SS and NS. However, the results possibly predicted post-surgical outcomes since all but one patient who underwent epilepsy surgery experienced neither seizure-freedom nor any significant decrease in seizures (Table 1). We considered the following three interpretations for the finding:

1. *The method was correct*: Both the mapping and mining showed distributed epileptic activity (not focused in the SOZ) for four patients who had Engel Class 4 outcomes. One seizure-free adult patient resumed medication after presurgical evaluation revealed multifocal onsets; interestingly, this patient had a somewhat even distribution of PGO-activity in SOZ/SS/NS (Fig. 6E) and the most connected PGO-activity in SOZ (Fig. 7E). In the one seizure-free postoperative patient, mapping and mining did not show PGO-activity solely in SOZ (cf. Figs. 6A and 7A) but this PGO-activity did occur in electrodes physically near the clinical SOZ (per D.D.) that were also resected. Each patient with poor postoperative outcome might have had a better Engel classification if the surgeon had included PGO-dense areas outside the clinical SOZ, such as ipsilateral PGOs near the SOZ.
2. *The method was limited*: This method analyzed only PGOs from a limited bandwidth of data (<100 Hz), which was the only available data for this study. The same analysis with another interictal epileptic discharge, such as pHFOs, might have produced different results. We considered that in future work must concurrently analyze both bandwidths (see ‘Relationship of PGO to pHFO’) for potentially complementary information about the SOZ and SS.
3. *The clinical SOZ was incomplete information*: The results of the method did not completely agree with the clinical presurgical evaluation. It was important to recall that the clinically marked SOZ albeit by a trained experienced neurologist was a subjective estimate of the true SOZ and EZ. Generally, for a human review to definitively predict the absolute SOZ, SS, and EZ was a difficult task and the accuracy of the estimate was not revealed until months after surgery. Only the clinical SOZ electrodes were excised for each patient, yet 4/5 patients had a poor post-surgical outcome. It would have been interesting to know the ensuing outcome if the extent of the resection had also included the electrodes with mapped or mined PGOs. Perhaps PGOs, or similar analysis of PGOs, might have helped identify the true SOZ in conjunction with other epileptic activity. Furthermore, when the mapping or mining identified interictal PGOs in electrodes outside the SOZ, it was possible that mechanisms of epileptic networks actually occurred in non-ictal or non-focal sites that were not readily discernible by a neurologist. Perhaps the clinical SOZ was a secondary site of pathology. Thus, the algorithmic PGO-analysis actually might have been more reliable information about the SOZ than the human markings or at minimum both types of markings were complementary information about a true epileptic network.

Additionally, we showed for most patients that varying the threshold each for the mapping or the mining (i.e., FIM support) produced a range of regions—changes in the distribution of activity in the SOZ, SS, and NS electrodes—that were frequently involved with PGOs. We supposed that the entire range represented the extent of the epileptogenic network while grouped electrodes at individual FIM supports within the range represented slices of the same epileptic network. Since the algorithm projected the partial or entire pathological network, it revealed a unique flexibility and usefulness in administering therapy.

Furthermore, we conjectured that the effects of a particular therapy (e.g., neurosurgery, medical device) depended upon which portion(s) of the network were treated.

4.3. Relationship of PGO to pHFO

The relationship of pathological gamma oscillations (<100 Hz) to pathological high-frequency oscillations (>100 Hz), such as ripples or fast ripples, is not currently clear. But lower frequency oscillations, such as PGOs, could potentially include some down-sampled components of higher frequency activity. Electrode size and geometry may also have significant effects on detecting pathological oscillations. Jirsch and others (Contreras & Steriade, 1996; Jirsch et al., 2007) reported that oscillations in the ripple (100–200 Hz) and fast ripple (200–500 Hz) ranges recorded from macro electrodes, when employed with high sampling-rate digitizers, were highly localized to primary epileptogenic regions and rarely localized to secondary regions of spread in patients with focal epilepsy. Worrell et al. using both standard and microelectrodes demonstrated that fast ripple oscillations were much more common around the seizure onset zone, though present in coupled regions, and were much better recorded with microelectrodes (Worrell et al., 2008). It is possible that analyzing PGOs regardless of the algorithm, geometric parameters of the electrode, or bandwidth of digitally acquired iEEG signals simply might not reveal the same information that a similar analysis with HFOs would reveal. But, on the other hand, it is also possible that an analysis of PGOs complements an analysis of HFOs to more completely accurately identify the epileptogenic network of a patient than either lone analysis. However, this hypothesis is also unclear until similar algorithms to map and mine epileptic networks analyze both interictal PGOs and interictal HFOs. We suppose that PGOs may play a slight individual role in ictogenesis, a role that could be more predictive in combination with other interictal epileptic discharges such as HFOs. Future studies should repeat this technique using a broadband dataset that may be analyzed in separate frequency-bands were each band contains a particular interictal epileptic discharge and should compare the results of each analysis.

4.4. Application for alternate therapy to neurosurgery

Ambulatory implantable therapeutic devices hold great promise for treating patients with medically refractory epilepsy who are not good candidates for resection. But as with neurosurgery, each novel medical device necessitates the localization of epileptic networks to determine where to sense abnormal activity and where to intervene, especially since these two locations might not necessarily be identical as observed in the presented results. The ability to define and characterize a network of brain-tissue that is involved in seizure generation or is required to modulate the process of seizure-generation is of increasing interest to clinicians, researchers, and the medical device industry. The presented methods may help guide the surgical implantation of electrodes for electrical pacemakers (Fisher et al., 2010; Fountas et al., 2005) or thermoelectric probes for focal cooling (Fujii et al., 2010).

5. Conclusion

Despite the limited (<100 Hz) bandwidth for commonly acquired clinical iEEG, long-duration multielectrode recordings are still useful to study and analyze. Ultimately, by combining a robust routine for detection with a proven procedure for mining, we discovered spatiotemporal patterns across multiple channels of long-duration EEG that may aid in pinpointing pathological brain regions for resection or placement of sensors and stimulation leads for implantable devices. We intend that results from the above framework can be used adjunctively by clinicians. We suspect that a network of coincident oscillations may not always completely co-localize with a clinically determined EZ and that objectively defining the EZ, such as using the presented technique, may provide additional useful evidence to

help guide surgical planning. However, we also anticipate that cases in which this framework reveals a noncontiguous or broadly spatially distributed network might also prove invaluable to clinicians as they decide for each patient the intended location and extent of surgical resection or delivered therapy from an implantable medical device.

Of course, the above hypotheses, particularly those focused on clinical applications, will require validation of our results in a larger number of patients. Nonetheless, our results present a proof-of-concept of a potential decision-support tool in presurgical evaluation. With further refinement these algorithms may become the foundation for novel technologies to clinically identify epileptic networks, improve the study of epilepsy, guide surgery or implantable therapeutic devices, and better treat patients with seizures.

Acknowledgments

6. Grants

This research was supported by funds from the National Institute of General Medical Sciences (IRACDA 5K12 GM000680-07) and the United Negro College Fund Special Programs Corporation (NASA Harriett G. Jenkins Pre-doctoral Fellowship Program) awarded to Dr. Smart and the National Institute of Neurological Disorders and Stroke (1R01NS048598-01A2), the Dana Foundation, the Epilepsy Research Foundation, and the Citizens United for Research in Epilepsy awarded to Dr. Litt.

We authors thanked Dr. Gregory Worrell for help in reviewing and marking PGOs and Dr. Brenda Porter for assistance in the information about the CHP patient.

References

Badier JM, Chauvel P. Spatio-temporal characteristics of paroxysmal interictal events in human temporal lobe epilepsy. Journal of Physiology – Paris. 1995; 89:255–264.

Bartolomei F, Wendling F, Bellanger JJ, Regis J, Chauvel P. Neural networks involving the medial temporal structures in temporal lobe epilepsy. Clinical Neurophysiology. 2001; 112:1746–1760. [PubMed: 11514258]

Bodon, F. A trie-based APRIORI implementation for mining frequent item sequences. Proceedings of the 1st international workshop on open source data mining: frequent pattern mining implementations; Chicago, Illinois: ACM; 2005. p. 56-65.

Bourien J, Bellanger JJ, Bartolomei F, Chauvel P, Wendling F. Mining reproducible activation patterns in epileptic intracerebral EEG signals: application to interictal activity. IEEE Transactions on Biomedical Engineering. 2004; 51:304–315. [PubMed: 14765703]

Bragin A, Engel J, Wilson CL, Fried I, Buzsaki G. High-frequency oscillations in human brain. Hippocampus. 1999; 9:137–142. [PubMed: 10226774]

Bragin A, Engel J, Wilson CL, Fried I, Mathern GW. Hippocampal and entorhinal cortex high-frequency oscillations (100–500 Hz) in human epileptic brain and in kainic acid-treated rats with chronic seizures. Epilepsia. 1999; 40:127–137. [PubMed: 9952257]

Bragin A, Mody I, Wilson CL, Engel J Jr. Local generation of fast ripples in epileptic brain. Journal of Neuroscience. 2002; 22:2012–2021. [PubMed: 11880532]

Bragin A, Wilson CL, Engel J Jr. Chronic epileptogenesis requires development of a network of pathologically interconnected neuron clusters: A hypothesis. Epilepsia. 2000; 41(Suppl 6):S144–S152. [PubMed: 10999536]

Bragin A, Wilson CL, Staba Richard J, Reddick M, Fried I, et al. Interictal high-frequency oscillations (80–500 Hz) in the human epileptic brain: Entorhinal cortex. Annals of Neurology. 2002; 52:407–415. [PubMed: 12325068]

Buzsaki G, Horvath Z, Urioste R, Hetke J, Wise K. High-frequency network oscillation in the hippocampus. Science. 1992; 256:1025–1027. [PubMed: 1589772]

Contreras D, Destexhe A, Steriade M. Spindle oscillations during cortical spreading depression in naturally sleeping cats. Neuroscience. 1997; 77:933–936. [PubMed: 9130774]

Contreras D, Steriade M. Spindle oscillation in cats: the role of corticothalamic feedback in a thalamically generated rhythm. [erratum appears in J Physiol (Lond) 1996 Mar 15;491(Pt 3):889.]. Journal of Physiology. 1996; 490:159–179. [PubMed: 8745285]

Destexhe A, Contreras D, Sejnowski TJ, Steriade M. Modeling the control of reticular thalamic oscillations by neuromodulators. NeuroReport. 1994; 5:2217–2220. [PubMed: 7881030]

Engel, J. Surgical treatment of the epilepsies. 1. Vol. 1. New York: Raven Press; 1987.

Engel J. Surgery for Seizures. New England Journal of Medicine. 1996; 334:647–653. [PubMed: 8592530]

Engel J Jr, Van Ness PC, Rasmussen TB, Ojemann LM. Outcome with respect to epileptic seizures. Surgical Treatment of the Epilepsies. 1993:609–621.

Esteller R, Echauz J, Tcheng T. Comparison of line length feature before and after brain electrical stimulation in epileptic patients. Conference Proceedings - IEEE Engineering in Medicine and Biology Society. 2004; 7:4710–4713.

Fisher R, Salanova V, Witt T, Worth R, Henry T, Gross R, et al. Electrical stimulation of the anterior nucleus of thalamus for treatment of refractory epilepsy. Epilepsia. 2010; 51:899–908. [PubMed: 20331461]

Fountas KN, Smith JR, Murro AM, Politsky J, Park YD, Jenkins PD. Implantation of a closed-loop stimulation in the management of medically refractory focal epilepsy: a technical note. Stereotactic and Functional Neurosurgery. 2005; 83:153–158. [PubMed: 16205108]

French JA, Kanner AM, Bautista J, Abou-Khalil B, Browne T, Harden CL, et al. Efficacy and tolerability of the new antiepileptic drugs II: Treatment of refractory epilepsy: Report of the Therapeutics and Technology Assessment Subcommittee and Quality Standards Subcommittee of the American Academy of Neurology and the American Epilepsy Society. Neurology. 2004; 62:1261–1273. [PubMed: 15111660]

Fujii M, Fujioka H, Oku T, Tanaka N, Imoto H, Maruta Y, et al. Application of focal cerebral cooling for the treatment of intractable epilepsy. Neurologia Medico-chirurgica. 2010; 50:839–844. [PubMed: 20885118]

Gardner AB, Worrell GA, Marsh E, Dlugos D, Litt B. Human and automated detection of high-frequency oscillations in clinical intracranial EEG recordings. Clinical Neurophysiology. 2007; 118:1134–1143. [PubMed: 17382583]

Jacobs J, LeVan P, Chander R, Hall J, Dubeau F, Gotman J. Interictal high-frequency oscillations (80–500 Hz) are an indicator of seizure onset areas independent of spikes in the human epileptic brain. Epilepsia. 2008; 49:1893–1907. [PubMed: 18479382]

Jirsch J, Chander R, Gotman J. Pre-ictal high frequency oscillations (100–450 Hz) in epileptogenic areas of patients with focal seizures. Epilepsia. 2007; 48:207.

Jirsch JD, Urrestarazu E, Levan P, Olivier A, Dubeau F, Gotman J. High-frequency oscillations during human focal seizures. Brain. 2006; 129:1593–1608. [PubMed: 16632553]

Kahane P, Merlet I, Gregoire MC, Munari C, Perret J, Mauguiere F. An H(2) (15)O-PET study of cerebral blood flow changes during focal epileptic discharges induced by intracerebral electrical stimulation. Brain. 1999; 122:1851–1865. [PubMed: 10506088]

Roederer M, Treister A, Moore W, Herzenberg LA. Probability binning comparison: A metric for quantitating univariate distribution differences. Cytometry. 2001; 45:37–46. [PubMed: 11598945]

Rosenow F, Luders H. Presurgical evaluation of epilepsy. Brain. 2001; 124:1683–1700. [PubMed: 11522572]

Spencer SS, Berg AT, Vickrey BG, Sperling MR, Bazil CW, Haut S, et al. Health-related quality of life over time since resective epilepsy surgery. Annals of Neurology. 2007; 62:327–334. [PubMed: 17567854]

Spencer SS, Berg AT, Vickrey BG, Sperling MR, Bazil CW, Shinnar S, et al. Initial outcomes in the multicenter study of epilepsy surgery. Neurology. 2003; 61:1680–1685. [PubMed: 14694029]

Staba RJ, Wilson CL, Bragin A, Fried I, Engel J Jr. Quantitative analysis of high-frequency oscillations (80–500 Hz) recorded in human epileptic hippocampus and entorhinal cortex. Journal of Neurophysiology. 2002; 88:1743–1752. [PubMed: 12364503]

Tanriverdi T, Ajlan A, Poulin N, Olivier A. Morbidity in epilepsy surgery: an experience based on 2449 epilepsy surgery procedures from a single institution. Journal of Neurosurgery. 2009; 110:1111–1123. [PubMed: 19199440]

Tanriverdi T, Poulin N, Olivier A. Life 12 years after temporal lobe epilepsy surgery: A long-term, prospective clinical study. Seizure. 2008; 17:339–349. [PubMed: 18083604]

Urrestarazu E, Chander R, Dubeau F, Gotman J. Interictal highfrequency oscillations (100–500 Hz) in the intracerebral EEG of epileptic patients. Brain. 2007; 130:2354–2366. [PubMed: 17626037]

Wiebe S, Blume WT, Girvin JP, Eliasziw M. A randomized, controlled trial of surgery for temporal-lobe epilepsy. New England Journal of Medicine. 2001; 345:311–318. [PubMed: 11484687]

Worrell GA, Gardner AB, Stead SM, Hu SQ, Goerss S, Cascino GJ, et al. High-frequency oscillations in human temporal lobe: simultaneous microwire and clinical macroelectrode recordings. Brain. 2008; 131:928–937. [PubMed: 18263625]

Worrell GA, Parish L, Cranstoun SD, Jonas R, Baltuch G, Litt B. Highfrequency oscillations and seizure generation in neocortical epilepsy. Brain. 2004; 127:1496–1506. [PubMed: 15155522]

Appendix A

A.1. Receiver operating characteristic curve and hypothesis testing for tuning detection

For each patient, we used the training dataset to design a robust high-performance detector for PGOs. We defined ‘robust’ to mean that subsequent analysis of detected events (i.e., mapping algorithm, mining algorithm) correctly returned an output despite the false positives or false negatives of the detector. We defined ‘high-performance’ as a minimal trade-off between sensitivity (Eq. A1) and selectivity (Eq. A2). Our condition for a robust detector was that the threshold resulted in no statistically significant difference between the median energy of true PGOs and the median energy of detected events. Our condition for a high-performance detector was that the threshold ranged between the saddle-point and point of peak selectivity on a receiver operating characteristic (ROC) curve in which the abscissae were measures of selectivity and the ordinates were measures of sensitivity. Thus, the overall analysis to design a detector combined a traditional ROC curve with hypothesis-testing—a test per point on the ROC curve—to estimate an appropriate rule (threshold) for detection (binary classification).

$$Sensitivity = \frac{numberoftruepositives}{numberoftrues + numberoffalsenegatives} \quad \text{(A1)}$$

$$Sensitivity = \frac{numberoftruepositives}{numberoftruepositives + numberoffalsepositives} \quad \text{(A2)}$$

To perform the analysis for each patient, we concatenated the training dataset to form a single segment of iEEG and compiled the corresponding manually marked time-stamps to form a single registry of time-stamps. We applied the automated detection at 100 distinct thresholds and computed the performance (i.e., both sensitivity and selectivity) of the detector at each threshold using the registry, resulting in a traditional ROC for a ‘conventional detector.’ Also, at each threshold we computed the energy of the actual PGOs (i.e., true positives and false negatives of the detector) and the detected events (i.e., true positives and false positives of the detector) for the single segment and executed a Mann-Whitney *U*-test (Wilcoxon rank-sum test), yielding a *p*-value for the similarity between the two independent samples. A *p*-value greater than or equal to 0.05 represented to a robust

threshold. To ultimately tune the detector, we chose a threshold that sufficed our two conditions for detection.

Appendix B

B.1. Frequent itemset mining

Frequent itemset mining (FIM) algorithms output frequent patterns in a collection of patterns, where the threshold for frequency is defined as a predetermined minimum likelihood for a pattern to occur. The following terms are used in FIM and help to explain its application in this study. A pattern is referred to as an *n-itemset*, or a set of n items, where an *item* a_k is some event of interest that is indexed by an integer k, $1 \le k \le n$. If a pattern is a subset of another pattern, it is termed that the latter pattern *contains* the latter pattern. A *database* Σ is a list of n-itemsets, or patterns, where each n-itemset may differ in the number of items, n, and $T = \Sigma$ is size of the database (or the total number of itemsets in Σ). Next, consider a specific itemset I within Σ. The *count* of I is the number of times that I occurs within Σ and is written as $count_{\Sigma}(I)$. The *support* of I is the fraction of itemsets in Σ that contain I, which is represented mathematically as

$$support_{\Sigma}(I) = \frac{count_{\Sigma}(I)}{T}, \quad 0 \le support_{\Sigma}(I) \le 1 \quad \text{(B1)}$$

Lastly, a λ-*frequent* n-itemset is an itemset I such that $support_{\Sigma}(I) \ge \lambda$, $0 \le \lambda \le 1$; and a *maximal* λ-*frequent* n-itemset is an itemset I such that $support_{\Sigma}(I') < \lambda$ for all I', where I' is an $(n + 1)$-itemset that contains I.

We apply FIM in the third primary analysis of our study. An item represents an electrode. An n-itemset is a group of electrodes that is obtained when the median energy within a particular 1-min window of detections exceeds a predefined threshold. The database is a catalog of grouped electrodes—one group per row (1-min interval) in Σ, and T is the number of 1-min intervals within the duration of the processed interictal record. A λ-frequent n-itemset signifies a group of n electrodes that occur at a minimum rate k within the interictal record, while the maximal (max) λ-frequent n-itemset signifies the most repetitive grouping of n electrodes in the same clip. For instance, the final stage of the automated localization may output a max *0.53*-frequent *6*-itemset with labels for electrodes in the right temporal lobe. That is, the processed multisite interictal iEEG reveals a repeated association of six electrodes in the right temporal lobe—each electrode exhibiting a relatively large amount of pathological energy—that occurs 53% of the time in iEEG before an impending seizure occurs.

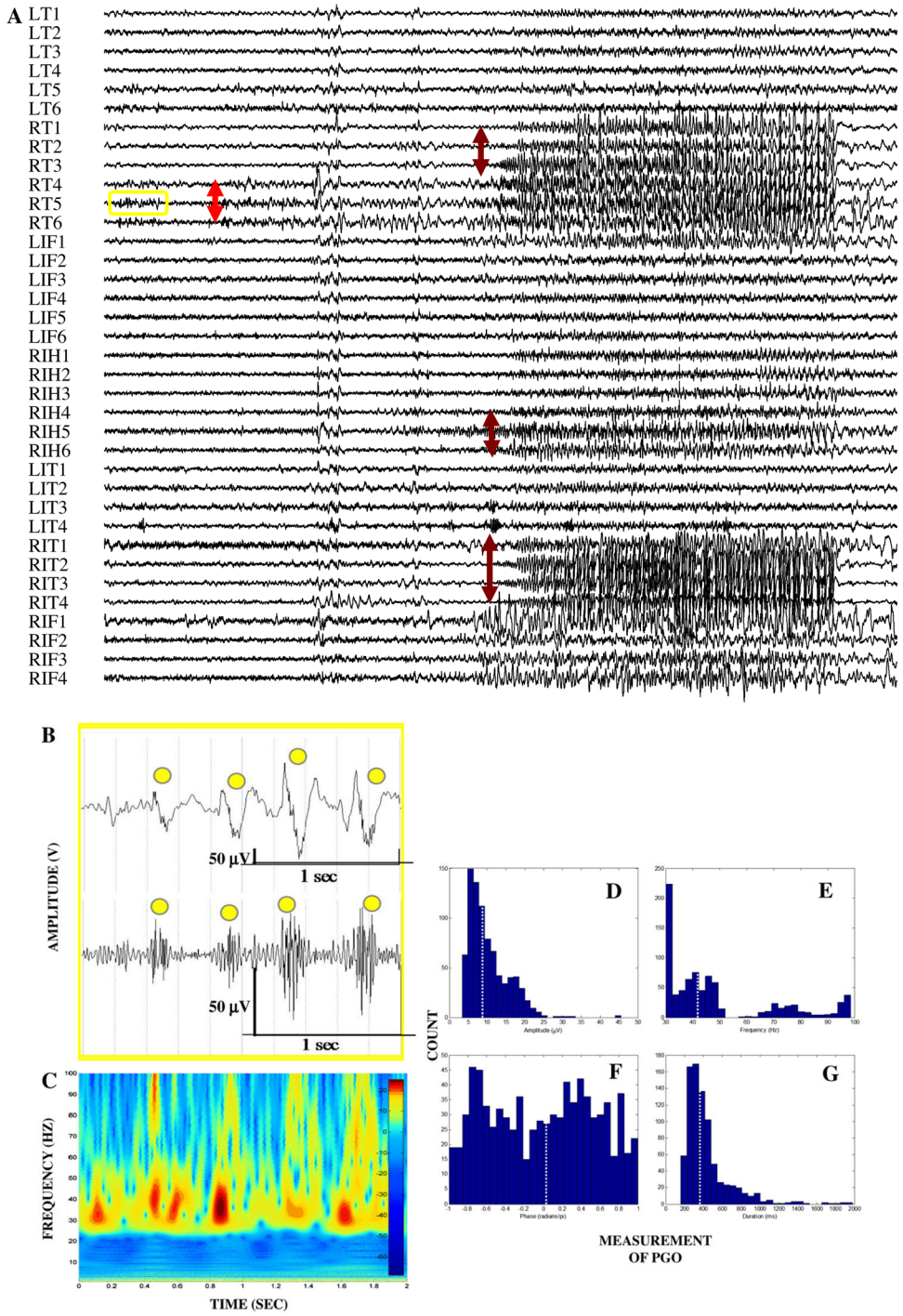

Fig. 1.

We analyzed interictal records in six patients with refractory epilepsy, such as the portions of iEEG seen here for Patient C. (A) For each interictal record, a clinician visually manually marked the SOZ independently from the objective semi-automated detection, mapping, and mining. For this patient, the seizures began in electrodes RT 4-6 (red arrow) before spreading to RT 1-3, RIT 1-4, and RIH 5-6 (dark red arrows). (B) A closer look at the interictal record (yellow box in A) revealed a few PGOs that occurred minutes before

seizure in the SOZ (top: unfiltered signal; bottom: filtered signal). (C) A time–frequency plot of the same activity in (B) using Wavelet analysis. (D–G) Histograms of the amplitude, frequency, phase, and duration of a sample (n = 1200) of marked in the training dataset for all six patients was also computed to quantitatively characterize the activity. (For interpretation of the references to colour in this figure legend, the reader is referred to the web version of this article.)

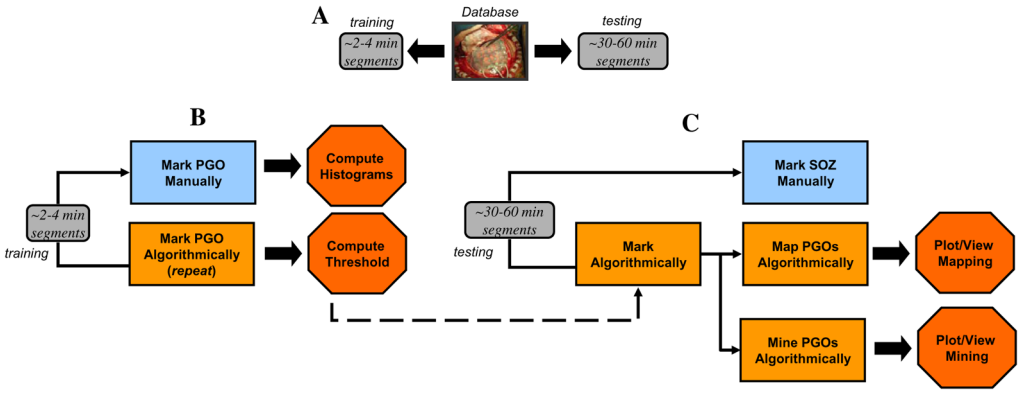

Fig. 2.

Schematic for the three primary analyses: (A) single-electrode short-duration clips of iEEG formed the training dataset and multi-electrode long-duration clips of iEEG formed the testing dataset; (B) Using the training dataset, a patient-specific threshold for the detector (detection) was computed. An epileptologist manually marked ‘gold standard’ PGOs before the semi-automated detector marked the same data at a several specific thresholds. The manual and automated marks were compared to compute an acceptable threshold for application to the long-term multichannel recordings. In addition, a sample of PGOs was taken from the training dataset so that histograms were computed after calculating four quantities of the PGOs (see Fig. 3); (C) The designed detector was applied to the testing dataset to estimate epileptic networks by mapping and mining PGOs. Subsequently, each result was visualized using an accordingly customized GUI. Also before executing the detector, an epileptologist marked the clinical SOZ. Ultimately, the SOZ was compared against each the mapped PGOs and the mined PGOs.

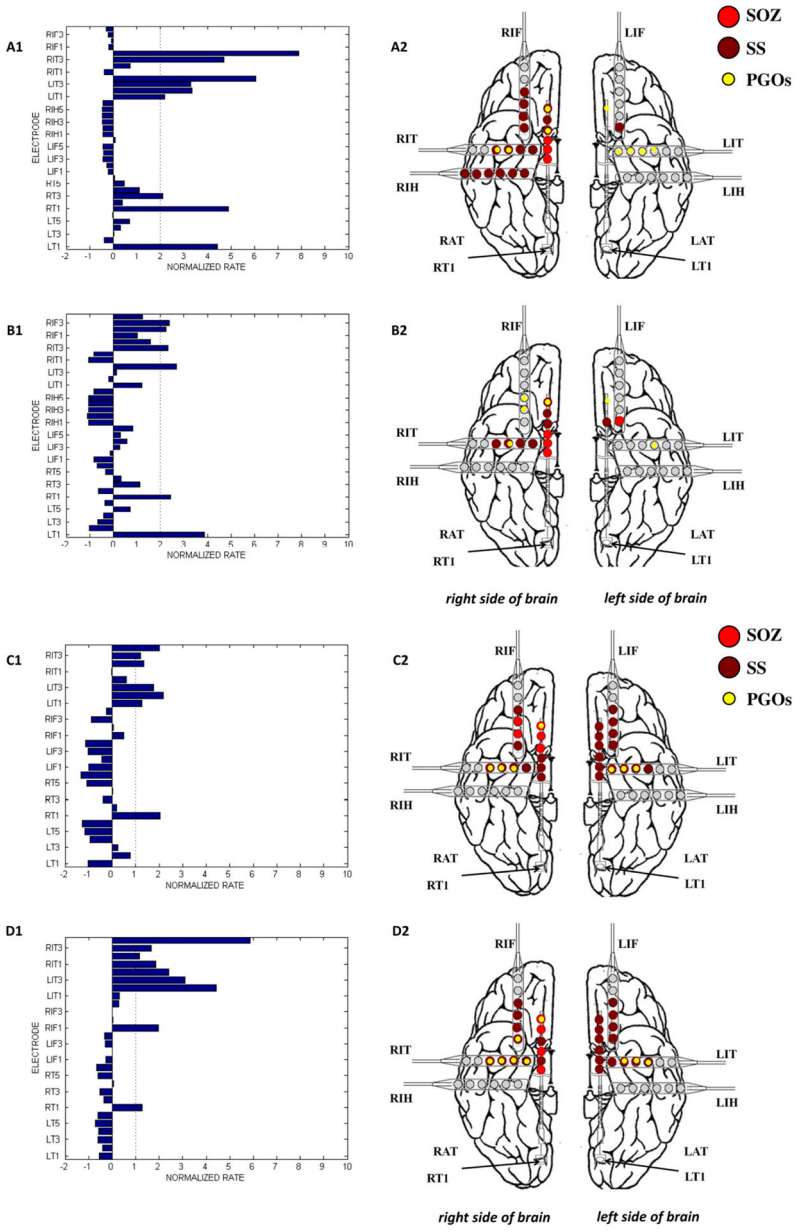

Fig. 3.

The results of the mapping algorithm for four selected interictal records from two patients. In these examples, mapping was executed with a threshold of 2.0 for the normalized rate of PGOs, but the threshold was varied from 0 to 6 for each interictal record. We plotted the mapped PGOs (small, yellow dots) using the PGO-rate measure, the marked SS (large, dark red dots) and the marked SOZ (large, red dots) on a template of an implanted human brain (A2, B2, C2, D2). We plotted a histogram of the measure, in this case the normalized rate of PGOs (*x*-axis) over the entire duration of the record per electrode (*y*-axis), which quantified the spatial distribution and density of PGOs in each interictal record (A1, B1, C1, D1). (For interpretation of the references to colour in this figure legend, the reader is referred to the web version of this article.)

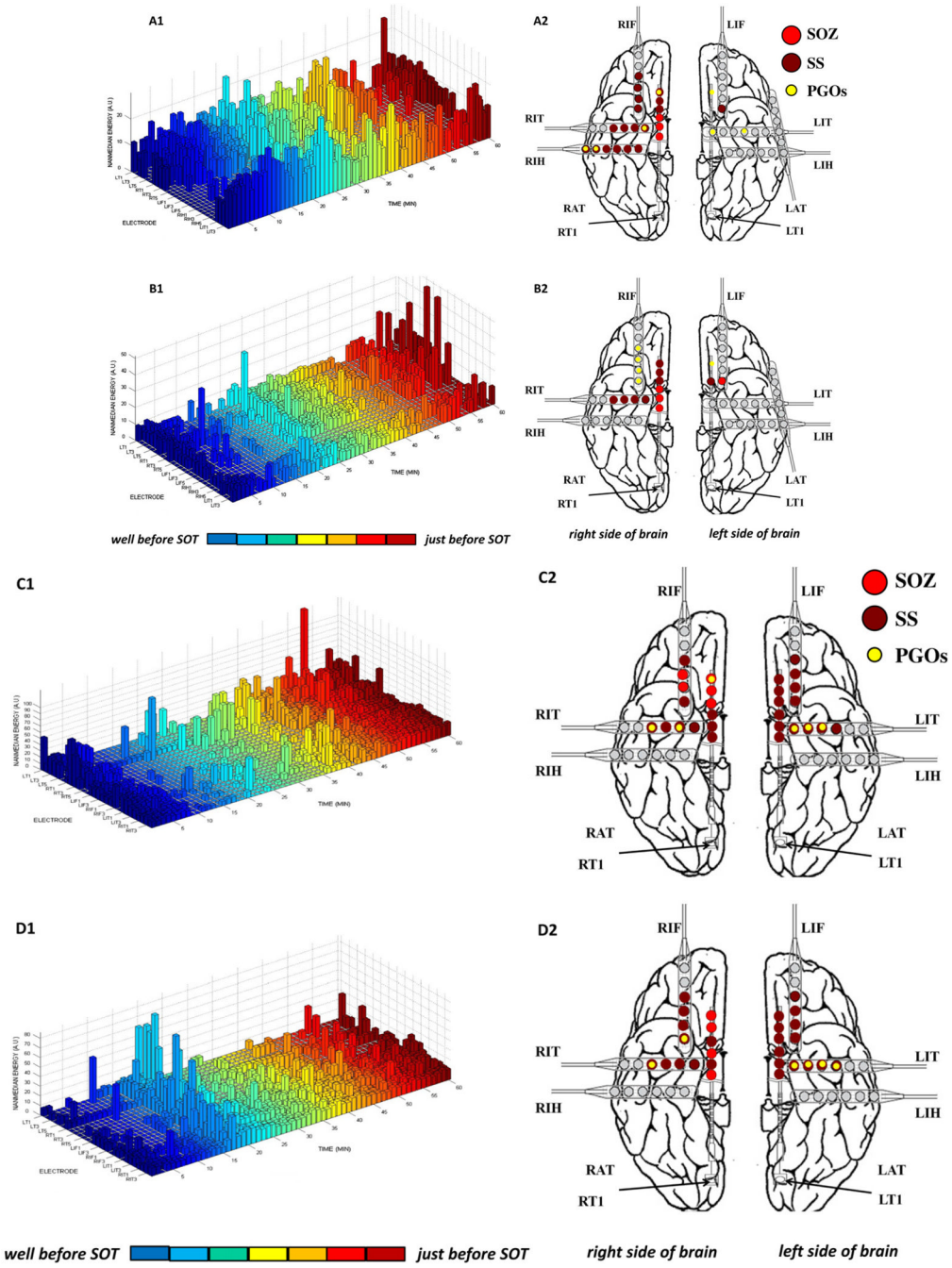

Fig. 4.

The results of the mining algorithm for four selected interictal records from two patients. Mining was executed with a support of 0.10—one cluster of electrodes per 6 min—in this example but the support was varied from 0.10 to 0.90 for each interictal record. We plotted the mined PGOs (small, yellow dots) using the PGO-rate measure, the marked SS (large, dark red dots) and the marked SOZ (large, red dots) on a template of an implanted human brain (A2, B2, C2, D2). We plotted the measure-matrix, in this case median energy of PGOs within 1-min non-overlapping time-window over the entire duration of the record per electrode, which quantified the spatial-temporal distribution and density of PGOs in each

interictal record (A1, B1, C1, D1). (For interpretation of the references to colour in this figure legend, the reader is referred to the web version of this article.)

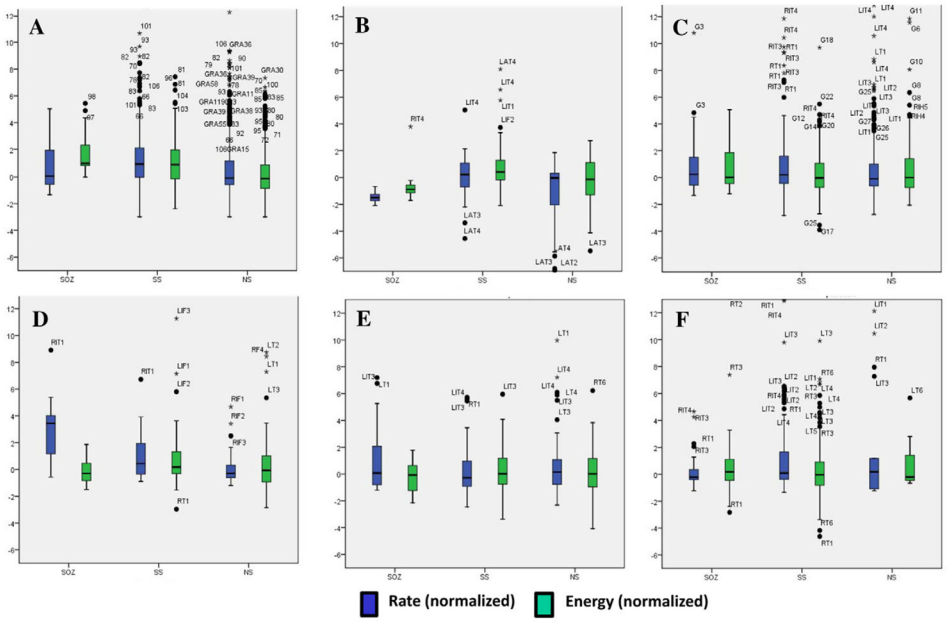

Fig. 5.

We compared the normalized PGO-rate (dark blue box-plots) and normalized median PGO-energy (light blue box-plots) across the SOZ, SS, and NS for each patient, including statistical outliers (black dot and label per specific iEEG electrode). (For interpretation of the references to colour in this figure legend, the reader is referred to the web version of this article.)

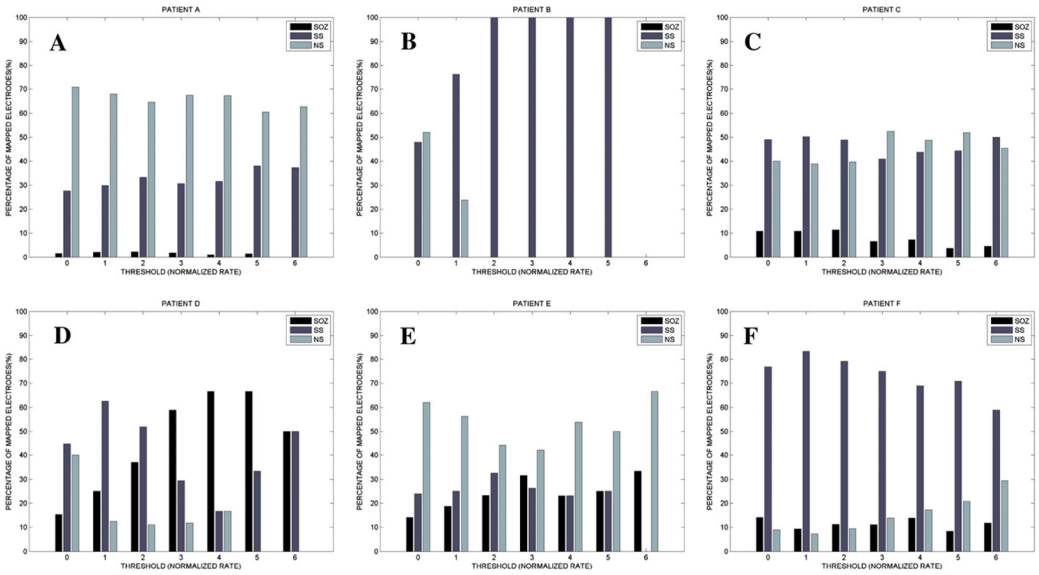

Fig. 6.

We computed the percentage of mapped electrodes by clinical label (i.e., SOZ, SS, NS). Each mapped electrode exceeded a threshold (value for normalized PGO-rate; higher value means higher rate) (*x*-axis) and was counted to compute the percentage (*y*-axis).

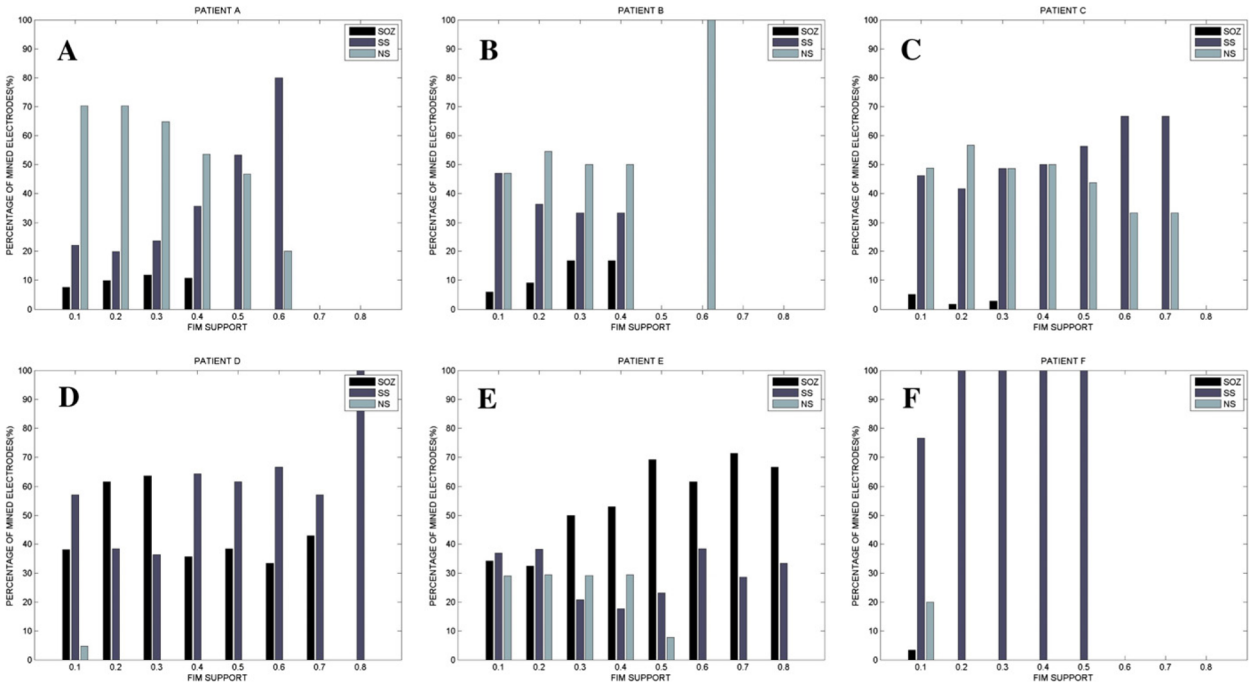

Fig. 7.

We computed the percentage of mined electrodes by clinical label (i.e., SOZ, SS, NS). Each mined electrode exceeded a threshold (value for consistency in connection between a group of electrodes with high normalized PGO-rates; higher value means more consistency) (*x*-axis) and was counted to compute the percentage (*y*-axis).

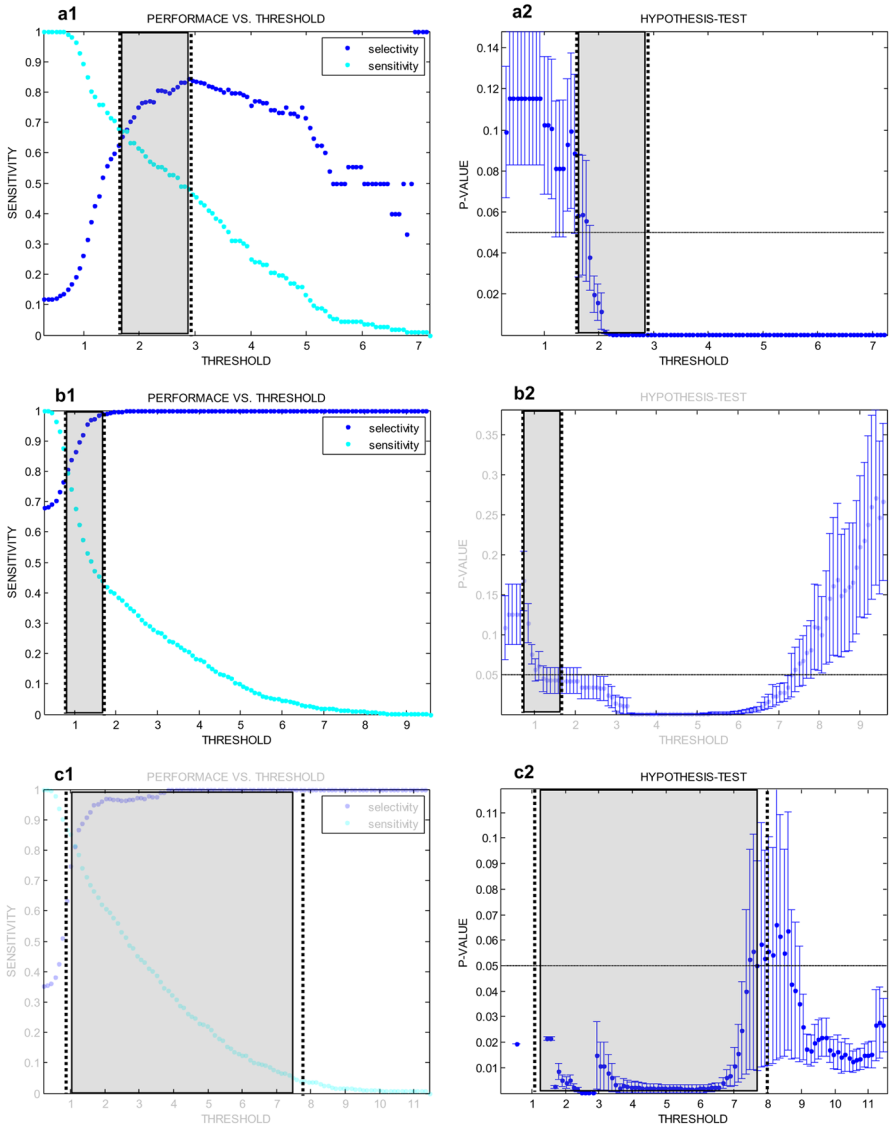

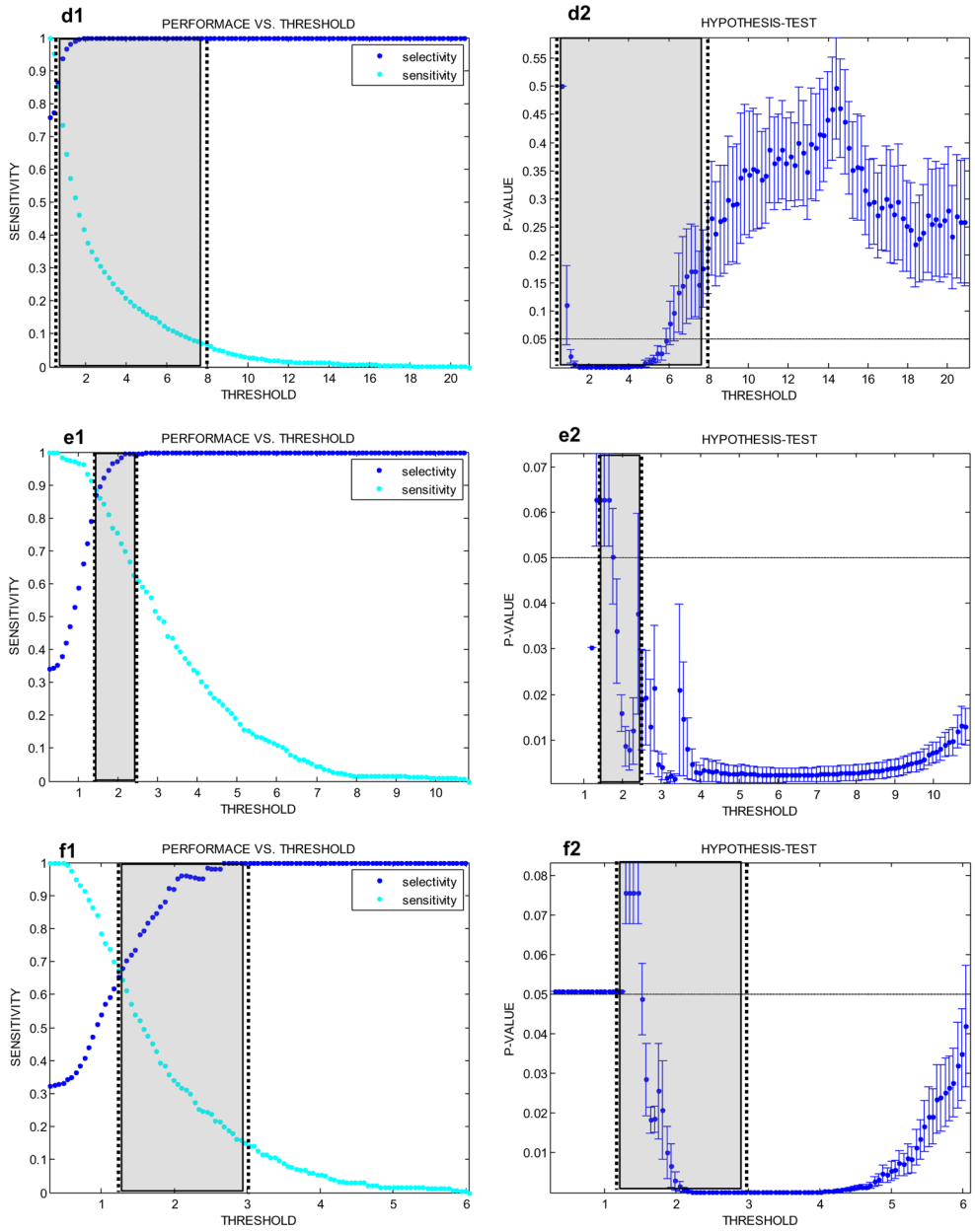

Fig. A1.

The hypothesis-tests with an ROC curve computed patient-specific thresholds for robustly detecting PGOs. For each point (threshold of the detector) of the ROC curve (top, blue points), the mean ± SD *p*-value (bottom, error-bars) was computed. The mean *p*-value quantified the projected robustness of the subsequent algorithm to localize epileptic networks from detected oscillations, despite inevitable false alarms and missed PGOs. We annotated the conventionally chosen threshold (top, arrow and black circled point6 and our selected threshold (bottom, dashed arrow over error-bar) for comparisons. (For interpretation of the references to colour in this figure legend, the reader is referred to the web version of this article.)

Table 1

We summarized the clinical data.

Patient	Age	Gender	Medical imaging	Electrodes	Clinical seizure onset zones	Surgery	Outcome 1 [months]	Outcome 1 [score]	Outcome 2 [years]	Outcome 2 [score]
A	9	M	FCD/lesion: R-AFL	RF, RP, RT	RF33-34 (C97-98)	R-AFL	12	1	8	1
B	56	F	Atrophy: MTL	LAT, LIT, LIF RIT, RIF	RIT4-5	R-ATL	18	4	12	4
C	53	F	Lesion: R-PFL, ACS	LT, LIF, LIT RT, RIF, RIT, RIH	RT4-6; G2-3,13-14	MST	12	4	9	4
D	21	M	Normal	LT, LIF, LIT, LF RT, RIF, RIT, RF	RIT1-2; RT2-3; LT4	R-ATL	27	4	6	4
LLJ	51	M	FCD: L-MH	LT, LIF, LIT RT, RIF, RIT	RIT1-4; LIT1-3 LT1-3; RIF1-3	*N/A*	*18*	*Seizures*	*13*	*Seizure-free*
F	42	F	Normal	LT, LIF, LIT RT, RIF, RIT	RT1-6; RIF2-4 RIT2-4	R-ATL	15	4	2	4

Abbreviations: left temporal (LT), right temporal (RT), left inferior temporal (LIT), right inferior temporal (RIT), left inferior frontal (LIF), right inferior frontal (RIF), left anterior temporal (LAT), right anterior temporal (RAT), left inferior hippocampus (LiH), right inferior hippocampus (RIH), grid (G), right anterior temporal lobectomy (R-ATL), multiple subpial transection (MST), not applicable (N/A), right posterior frontal lobe (R-PFL), anterior central sulcus (ACS), mesial temporal lobe (MTL), focal cortical dysplasia (FCD), right anterior frontal lobe (R-AFL), and left medial hippocampus (L-MH).

Notes: Patient A was implanted with 126 total electrodes (C1-126) using four grids and two strips in the right frontal (RF), right parietal (RP), and right temporal (RT) lobes. Only patients C and D were implanted with RIH electrodes while only patient D was implanted with LiH electrodes. Patient C was also implanted with 28 grid electrodes (G1-28) in the right frontal lobe. Patient E did not have surgery because of clinically determined multifocal onsets but medication eventually lead to seizure-freedom after initial seizures. Outcomes were measured after surgery except for Patient E (outcome was measured after end of video-iEEG monitoring in EMU).

Table A1

We performed both a standard ROC and a probabilistic ROC (pROC) analyses (‘see Appendix’) to compute patient-specific thresholds for the detecting PGOs.

		Conventional tuning			Robust tuning			
Patient	**AUC**	**Selectivity**	**Sensitivity**	**Threshold[a]**	**Selectivity**	**Sensitivity**	**Threshold[a]**	***p*-value (mean ± SE)**
A	0.565	0.764	0.607	2.046	0.676	0.670	1.766	0.056 ± 0.030
B	0.913	0.692	0.992	0.457	0.897	0.625	1.115	0.061 ± 0.018
C	0.888	0.866	0.784	1.231	1.000	0.046	7.586	0.055 ± 0.046
D	0.951	0.758	1.000	0.235	0.936	0.733	0.860	0.110 ± 0.070
E	0.950	0.924	0.842	1.642	0.947	0.812	1.749	0.050 ± 0.011
F	0.758	0.653	0.675	1.231	0.737	0.539	1.463	0.075 ± 0.008

[a]Thresholds for both analyses were computed in arbitrary units (a.u.). The mean *p*-value for each pROC was computed as the sample mean ± SE in sample mean.